

Coordination Control of Intramolecular Electron Transfer in Boronate-Bridged Zinc Porphyrin–Diimide Molecules

Hideo Shiratori,[†] Takeshi Ohno,[‡] Koichi Nozaki,[‡] Iwao Yamazaki,[§]
Yoshinobu Nishimura,[§] and Atsuhiko Osuka^{*,†}

Department of Chemistry, Graduate School of Science, Kyoto University, Kyoto 606-8502, Japan,
Department of Chemistry, Graduate School of Science, Osaka University, Toyonaka 560-8531, Japan, and
Department of Chemical Process Engineering, Graduate School of Engineering, Hokkaido University,
Sapporo 060-8268, Japan

osuka@kuchem.kyoto-u.ac.jp

Received August 23, 2000

Three sets of dyads, in which a zinc–porphyrin (ZP) electron donor is connected to an aromatic diimide electron acceptor, either pyromellitimide (PI) or naphthalene-1,8:4,5-tetracarboxylic acid diimide (NI), via a boronate-ester bridge, a piperidine bridge, and a 1,3-dioxolane bridge, respectively, were prepared for the purpose of control of intramolecular electron transfer (ET) by acid–base reactions at the connecting bridge. Boronate–ester bridge is a Lewis acidic site and confers a chance to regulate intramolecular ET reaction upon base coordination. This has been demonstrated by suppression of photoinduced ET from ZP to PI or NI in highly electron-pair donating solvents or upon addition of a fluoride anion. To extend this strategy to control of ET-path selectivity, we prepared triad **18**, which consists of a ZP donor bearing NI and PI acceptors at similar distances through a boronate–ester bridge and an acetal bridge, respectively. Photoexcitation of **18** in a free form led to intramolecular ET from ¹ZP* preferentially to NI, but the ET path was completely switched toward PI in F[−]-coordinated form without a serious drop in the rate, constituting a novel ET-switching molecular system.

Introduction

In recent years, intramolecular electron transfer (ET) has been the subject of intense studies that are aimed at elucidating the role of the various parameters that govern ET rate.^{1–3,18} Among these, the electronic properties of a bridge connecting a donor and an acceptor are

important, since ET reactions can be facilitated by appropriate molecular orbitals provided by the bridge.^{2,3} A number of covalently linked donor–acceptor models have been developed to prove the effectiveness of the intervening spacer in mediating electronic interactions between donor and acceptor.^{2,4} When a donor–acceptor

[†] Kyoto University.

[‡] Osaka University.

[§] Hokkaido University.

(1) (a) Kavarnos, G. J.; Turro, N. *J. Chem. Rev.* **1986**, *86*, 401. (b) Wasielewski, M. R. *Chem. Rev.* **1992**, *92*, 435. (c) Sessler, J. L. *Israel J. Chem.* **1992**, *32*, 449. (d) Gust, D.; Moore, T. A.; Moore, A. L. *Acc. Chem. Res.* **1993**, *26*, 198. (e) Kurreck, H.; Huber, M. *Angew. Chem., Int. Ed. Engl.* **1995**, *34*, 849.

(2) (a) Paddon-Row: M. N.; Verhoeven, J. W. *New J. Chem.* **1991**, *15*, 107. (b) Closs, G. L.; Johnson, M. D.; Miller, J. R.; Piotrowiak, P. *J. Am. Chem. Soc.* **1989**, *111*, 3751. (c) Joran, A. D.; Leland, B. A.; Geller, G. G.; Hopfield, J. J.; Dervan, P. B. *J. Am. Chem. Soc.* **1984**, *106*, 6090. (d) Davis, W. B.; Svec, W. A.; Ratner, M. A.; Wasielewski, M. R. *Nature* **1998**, *396*, 60.

(3) (a) McConnell, H. M. *J. Chem. Phys.* **1961**, *35*, 508. (b) Larsson, S. *J. Am. Chem. Soc.* **1981**, *103*, 4034. (c) Newton, M. D. *Chem. Rev.* **1991**, *91*, 767. (d) Newton, M. D. *J. Electroanal. Chem.* **1997**, *438*, 3. (e) Paddon-Row: M. N. *Acc. Chem. Res.* **1994**, *27*, 18. (f) Hayashi, S.; Kato, S. *J. Phys. Chem.* **1998**, *102*, 2878. (g) Hush, N. S. *Coord. Chem. Rev.* **1985**, *64*, 135. (h) Penfield, K. W.; Miller, J. R.; Paddon-Row: M. N.; Cotsaris, E.; Oliver, A. M.; Hush, N. S. *J. Am. Chem. Soc.* **1987**, *109*, 5061. (i) Chambron, J.-C.; Harriman, A.; Heitz, V.; Savauge, J.-P. *J. Am. Chem. Soc.* **1993**, *115*, 5, 7415.

(4) (a) Osuka, A.; Tanabe, N.; Kawabata, S.; Yamazaki, I.; Nishimura, Y. *J. Org. Chem.* **1995**, *60*, 7177. (b) Osuka, A.; Maruyama, K.; Mataga, N.; Asahi, T.; Yamazaki, I.; Tamai, N. *J. Am. Chem. Soc.* **1990**, *112*, 4958. (c) Osuka, A.; Kobayashi, F.; Maruyama, K.; Mataga, N.; Asahi, T.; Okada, T.; Yamazaki, I.; Nishimura, Y. *Chem. Phys. Lett.* **1993**, *201*, 223. (d) Helm, A.; Heller, D.; McLendon, G. *J. Am. Chem. Soc.* **1992**, *114*, 6227. (e) Verhoeven, J. W. *Pure Appl. Chem.* **1986**, *58*, 1285. (f) Benniston, A. C.; Gouille, V.; Harriman, A.; Lehn, J.-M.; Marczinke, B. *J. Phys. Chem.* **1994**, *98*, 7794. (g) Harriman, A.; Ziesse, R. *Chem. Commun.* **1996**, 1707. (h) Würthner, F.; Vollmer, M. S.; Effenberger, F.; Emele, P.; Meyer, D. U.; Port, H.; Wolfe, H. C. *J. Am. Chem. Soc.* **1995**, *117*, 8090.

(5) Preliminary reports, see: (a) Shiratori, H.; Ohno, T.; Nozaki, K.; Yamazaki, I.; Nishimura, Y.; Osuka, A. *Chem. Commun.* **1998**, 1539. (b) Shiratori, H.; Ohno, T.; Nozaki, K.; Osuka, A. *Chem. Commun.* **1999**, 2181.

(6) Toi, H.; Nagai, Y.; Aoyama, Y.; Kawabe, H.; Aizawa, K.; Ogoshi, H. *Chem. Lett.* **1993**, 1043.

(7) Osuka, A.; Nagata, T.; Kobayashi, F.; Maruyama, K. *J. Heterocycl. Chem.* **1990**, *27*, 1657.

(8) Osuka, A.; Marumo, S.; Wada, Y.; Yamazaki, I.; Yamazaki, T.; Shirakawa, Y.; Nishimura, Y. *Bull. Chem. Soc. Jpn.* **1995**, *68*, 2909.

(9) Koreeda, M.; Luengo, J. I. *J. Org. Chem.* **1984**, *49*, 2081.

(10) (a) Wolfe, J. P.; Buchwald, S. L. *J. Org. Chem.* **1997**, *62*, 1264.

(b) Louie, J.; Driver, M. S.; Hamann, B. C.; Hartwig, J. F. *J. Org. Chem.* **1997**, *62*, 1268.

(11) Osuka, A.; Tanabe, N.; Nakajima, S.; Maruyama, K. *J. Chem. Soc., Perkin Trans. 2* **1995**, 199.

(12) (a) Osuka, A.; Nakajima, S.; Maruyama, K.; Mataga, N.; Asahi, T.; Yamazaki, I.; Nishimura, Y.; Ohno, T.; Nozaki, K. *J. Am. Chem. Soc.* **1993**, *115*, 4577. (b) Osuka, A.; Zhang, R.-P.; Maruyama, K.; Mataga, N.; Tanaka, Y.; Okada, T. *Chem. Phys. Lett.* **1993**, *215*, 179.

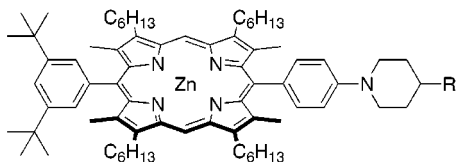
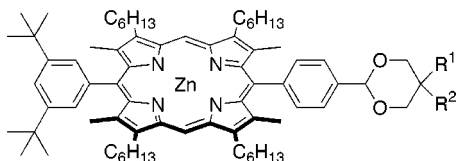
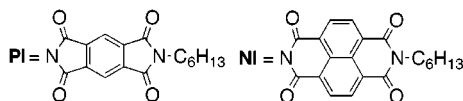
(c) Wiederrecht, G. P.; Niemczyk, M. P.; Svec, W. A.; Wasielewski, M. R. *J. Am. Chem. Soc.* **1996**, *118*, 81.

(13) (a) Gutmann, V. *Coord. Chem. Rev.* **1967**, *2*, 239. (b) Gutmann, V. *Electrochim. Acta* **1976**, *21*, 661.

(14) Udo, W.; Sakaguchi, Y.; Hayashi, H.; Nohya, G.; Yonoshima, R.; Nakajima, S.; Osuka, A. *J. Phys. Chem.* **1995**, *99*, 13930.

(15) (a) Deisenhofer, J.; Norris, J. R. *The Photosynthetic Reaction Center*; Academic Press: New York, 1993 (b) Woodbury, N.; Allen, J. P. *Anoxygenic Photosynthetic Bacteria*; Blankenship, R. E.; Madigan, M. T.; Bauer, C. E., Eds.; Kluwer Academic Publishers: Dordrecht, 1995. (c) Chan, C.-K.; Chen, L. X.-Q.; DiMaggio, T. J.; Nance, S. L.; Schiffer, M.; Norris, J. R. *Chem. Phys. Lett.* **1991**, *176*, 366. (d) Heller, B. A.; Holten, D.; Kirmaier, C. *Science* **1995**, *269*, 940.

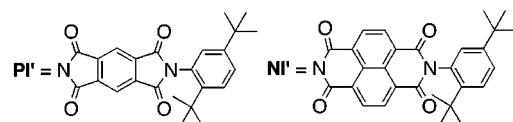
(16) All semiempirical MO calculations were performed by using MOPAC 97 (AM1) on Chem3D Pro (version 5.0, CambridgeSoft Co.).

Chart 1. Model Compounds 1 (B-bridged), 2 (N-bridged), and 3 (C-bridged)**1a**; R¹, R² = CH₃**1b**; R¹ = H, R² = PI**1c**; R¹ = H, R² = NI**2a**; R = H**2b**; R = PI**2c**; R = NI**3a**; R¹, R² = CH₃**3b**; R¹ = H, R² = PI**3c**; R¹ = H, R² = NI

molecule undergoes an intramolecular ET reaction tunable by external physical and/or chemical input, it may constitute a switching ET molecular system. Such ET systems will be quite useful as a switching component of supramolecular devices. We report here intramolecular photoinduced electron transfer in boronate-ester bridged zinc-porphyrin (ZP)-pyromellitimide (PI) **1b** and zinc-porphyrin (ZP)-1,8:4,5-naphthalene-tetracarboxylic diimide (NI) **1c** (Chart 1) in which the Lewis acidic boronate ester confers a chance to tune intramolecular ET rate upon base coordination. This has indeed been demonstrated by ET-suppression upon an addition of a fluoride anion (F⁻) at the boronate bridge.⁵ The piperidine bridge is basic and may be protonated with suitable acids. Here we also examined the possibility of control of intramolecular ET over a piperidine bridge by using models **2b** and **2c**. 1,3-Dioxolane-bridged compounds **3b** and **3c** were prepared as reference molecules.

(17) (a) Mataga, N. In *Electron Transfer in Inorganic, Organic, and Biological Systems*; Bolton, J. R., Mataga, N., McLendon, G., Eds.; Advances in Chemistry Series 228; American Chemical Society: Washington, DC, 1991; pp 91–115. (b) Kakitani, T.; Yoshimori, A.; Mataga, N. In *Electron Transfer in Inorganic, Organic, and Biological Systems*; Bolton, J. R., Mataga, N., McLendon, G., Eds.; Advances in Chemistry Series 228; American Chemical Society, Washington, DC, 1991; pp 45–69. (c) Asahi, T.; Ohkohchi, M.; Matsusaka, R.; Mataga, N.; Zhang, R. P.; Osuka, A.; Maruyama, K. *J. Am. Chem. Soc.* **1993**, *115*, 5665. (d) Heitele, H.; Pöllinger, F.; Häberle, T.; Michel-Beyerle, M. E.; Staab, H. A. *J. Phys. Chem.* **1994**, *98*, 7402–7410. (e) Joran, A. D.; Leland, B. A.; Felker, P. M.; Zewell, A. H.; Hopfield, J. J.; Dervan, P. B. *Nature* **1987**, *107*, 1080–1082.

(18) (a) Marcus, R. A.; Sutin, N. *Biochim. Biophys. Acta* **1985**, *811*, 265. (b) Grampp, G. *Angew. Chem., Int. Ed. Engl.* **1993**, *32*, 691. (c) Marcus, R. A. *Angew. Chem., Int. Ed. Engl.* **1993**, *32*, 1111.

Chart 2. Triad Model 18 and Its Reference Molecules**18**; R¹, R³ = H, R² = PI', R⁴ = NI'**19**; R¹, R² = CH₃, R³ = H, R⁴ = NI'**20**; R¹ = H, R² = PI', R³, R⁴ = CH₃**21**; R¹, R², R³, R⁴ = CH₃

Results

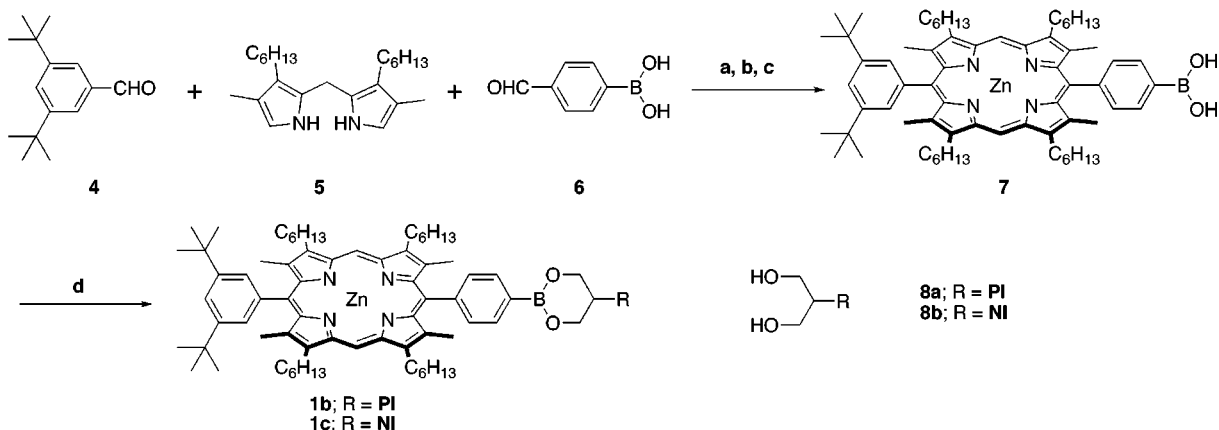
Synthesis. Boronate-ester appended zinc porphyrin **1a** was prepared according to the method reported by Toi et al.⁶ Attempted hydrolysis of the boronate ester of **1a** was unsuccessful in our hands under both the acidic and basic conditions. Synthesis of the boronate-ester bridged (B-bridged) models **1b** and **1c** is shown in Scheme 1. Porphyrinboronic acid **7** was prepared by cross-condensation^{7,12a} of 3,5-di-*tert*-butylbenzaldehyde (**4**) and 4-formylphenylboronic acid (**6**) with dipyrromethane **5** in a mixture of CH₂Cl₂ and acetonitrile followed by oxidation with *p*-chloranil under mild conditions (0 °C, 30 min) in 35% yield. The dyads **1b** and **1c** were prepared by refluxing a toluene solution of **7** in the presence of diimide-appended diol **8a** or **8b**⁸ in 84 and 90% yields, respectively.

Synthesis of the piperidine-bridged (N-bridged) models **2a–c** is shown in Scheme 2. Initially, the primary amino group of 4-amino-1-benzylpiperidine was protected with phthalic anhydride by refluxing in DMF, and then the benzyl substituent was cleaved by heating in the presence of 1-chloroethyl chloroformate followed by refluxing in methanol,⁹ to provide **10**. Pd-catalyzed coupling of **10** with bromide **11** under the recently improved conditions¹⁰ gave **12b** in 30% yield. After deprotection of the acetal group under acidic conditions, aldehyde **13b** was condensed with **4** and **5** to afford porphyrin **14** in 24% yield. The phthaloyl protecting group in **14** was cleaved with hydrazine in a mixture of ethanol and THF under mild conditions (room temperature, 18 h) to give aminoporphyrin **15**. Condensation of **15** with imide-anhydride **16a** or **16b** in refluxing pyridine to give **2b** and **2c** in 84 and 87% yields, respectively. Piperidine-appended reference porphyrin **2a** was prepared via a similar route.

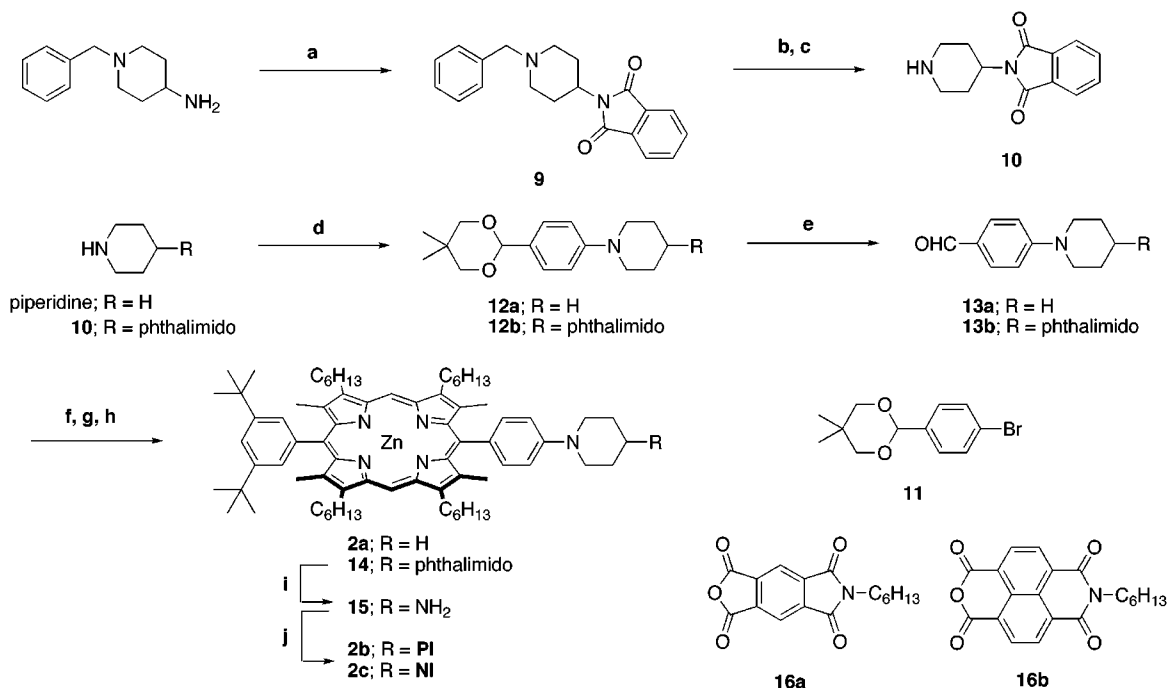
Synthesis of porphyrins **3a** and **17** was reported elsewhere.¹¹ Acetal condensation of formyl-substituted porphyrin **17** with diimide-appended diol **8a** or **8b** in the presence of an excess amount (50 equiv) of pyridinium *p*-toluenesulfonate (PPTS)⁸ gave the C-bridged dyads **3b** and **3c** in 78 and 34% yields, respectively (Scheme 3).

Synthetic procedures of **18–21** are shown in Schemes 4 and 5. Acid-catalyzed acetal condensation of diimide-appended diol **22** with terephthalaldehyde gave PI'-appended benzaldehyde **23** in 89% yield. A bulky 2,5-di-*tert*-butylphenyl substituent was introduced in order to improve the solubility of **23**. Cross condensation⁷ of **23** and **6** with **5** in the presence of trichloroacetic acid

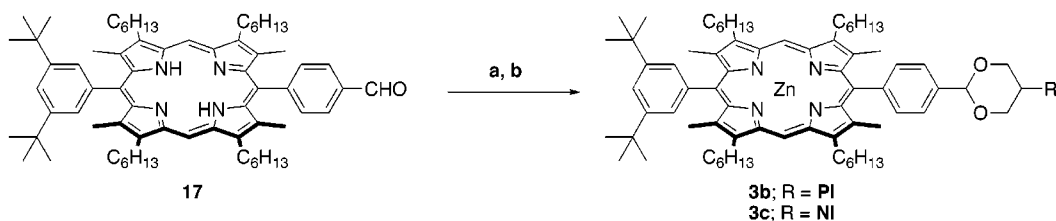
Scheme 1. Synthesis of 1b and 1c



Scheme 2. Synthesis of 2b and 2c



Scheme 3. Synthesis of 3b and 3c



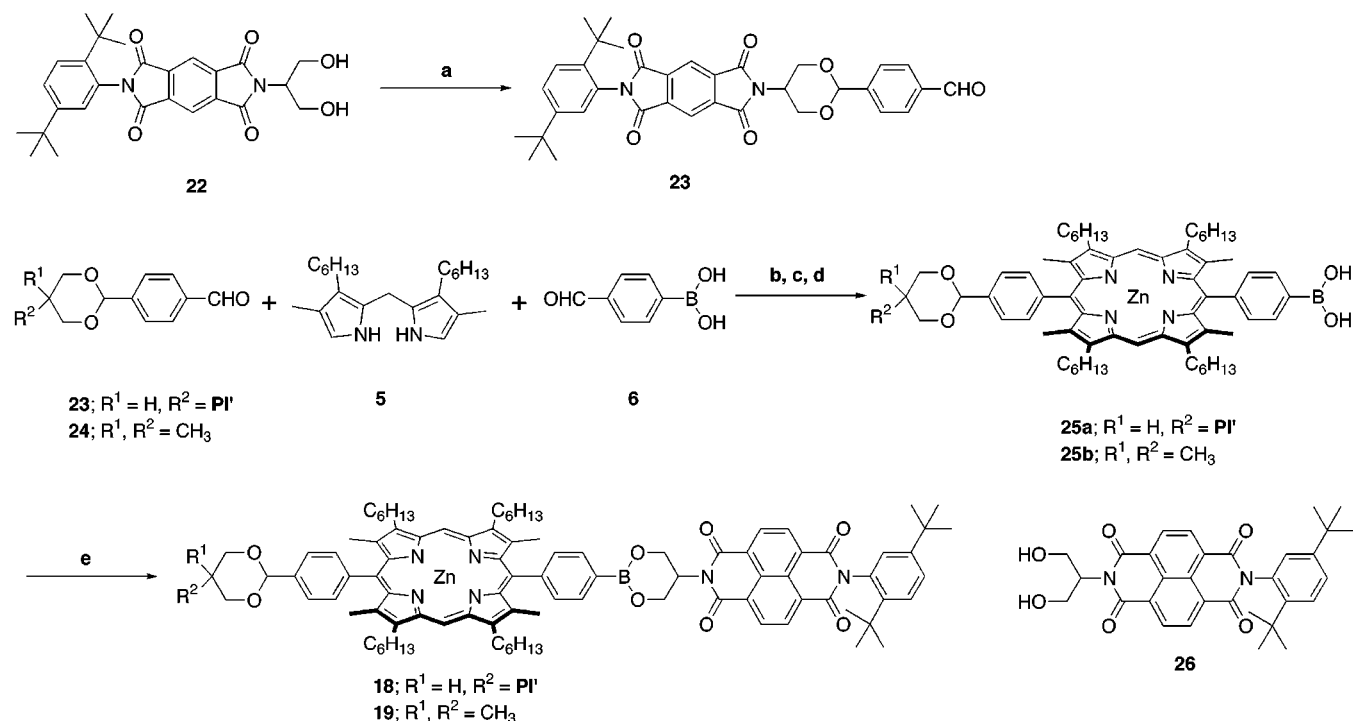
followed by *p*-chloranil oxidation gave porphyrin **25a** in 25% yield. Triad **18** was prepared by refluxing a toluene solution of **25a** in the presence of NI'-appended diol **25** in 76% yield. Dyads **19** and **20** and diimide-free compound **21** were prepared via the similar route.

All new compounds were fully characterized by ¹H NMR spectra and FAB or MALDI-TOF mass spectra.

Steady-State Absorption and Fluorescence Spectra. UV-vis absorption spectra of **1a–c** taken in benzene are shown in Figure 1a. Except the additional absorbance below 400 nm due to the NI subunit in **1c**, the three spectra are the same, indicating that the electronic interactions between chromophores are negligible in the

ground state. Absorption spectra of **2a–c** and **3a–c** are nearly the same as those of **1a–c**. The absorption spectra of these molecules were also examined in a wide range of solvents including CH₂Cl₂, THF, DMF, benzonitrile, pyridine, and triethylamine. In all the solvents examined, the absorption spectra are essentially the simple sum of the corresponding chromophores, indicating that the electronic interactions between chromophores are negligible in the ground state. In coordinating basic solvents such as pyridine and triethylamine, the absorption spectra of the B-bridged models are quite similar to those of the N-bridged models and C-bridged models, suggesting that the interaction of Lewis acidic boronate-ester

Scheme 4. Synthesis of 18 and 19



Scheme 5. Synthesis of 20 and 21

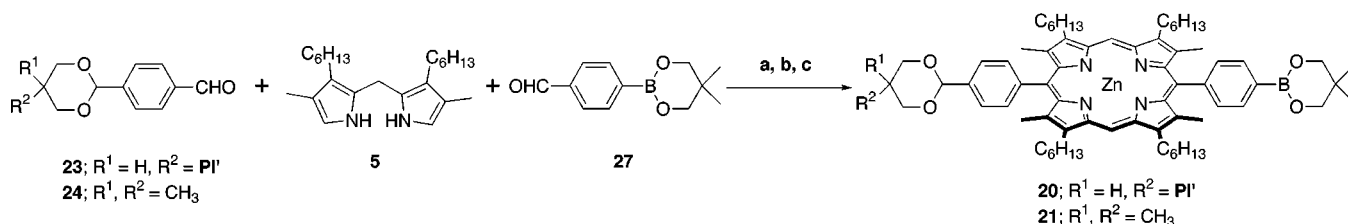


Table 1. Solvent Effects on the Fluorescence Properties of Dyads: (*I*/*I*₀), Relative Fluorescence Intensity; *k*_{CS}, Calculated CS Rate

solvent	ε ^a	DN ^b	AN ^c	<i>I</i> / <i>I</i> ₀ ^d (<i>kCS</i> / <i>s</i> ⁻¹) ^e					
				1b	1c	2b	2c	3b	3c
benzene	2.28	0.1	8.2	0.70 (3.1 × 10 ⁸)	0.36 (1.3 × 10 ⁹)	0.62 (4.4 × 10 ⁸)	0.34 (1.4 × 10 ⁹)	0.89 (9.2 × 10 ⁷)	0.36 (1.3 × 10 ⁹)
CH ₂ Cl ₂	8.93	—	20.4	0.75 (2.4 × 10 ⁸)	0.54 (6.0 × 10 ⁸)	0.64 (4.1 × 10 ⁸)	0.43 (9.4 × 10 ⁸)	0.88 (1.0 × 10 ⁸)	0.54 (6.1 × 10 ⁸)
THF	7.58	20.0	16.0	0.83 (1.5 × 10 ⁸)	0.54 (6.1 × 10 ⁸)	0.65 (3.8 × 10 ⁸)	0.41 (1.0 × 10 ⁹)	0.93 (5.5 × 10 ⁷)	0.49 (7.4 × 10 ⁸)
DMF	36.1	26.6	15.5	1.01 (—)	1.00 (—)	0.66 (3.7 × 10 ⁸)	0.45 (8.6 × 10 ⁸)	0.93 (5.1 × 10 ⁷)	0.57 (5.5 × 10 ⁸)
benzonitrile	25.2	11.9	8.0	0.71 (2.9 × 10 ⁸)	0.47 (8.1 × 10 ⁸)	0.64 (4.0 × 10 ⁸)	0.39 (1.1 × 10 ⁹)	0.83 (1.4 × 10 ⁸)	0.42 (9.9 × 10 ⁸)
pyridine	12.4	33.1	14.2	0.99 (—)	0.99 (—)	0.60 (4.8 × 10 ⁸)	0.36 (1.3 × 10 ⁹)	0.85 (1.3 × 10 ⁸)	0.41 (1.0 × 10 ⁹)
triethylamine	2.4	61.0	—	1.00 (—)	0.99 (—)	0.54 (6.0 × 10 ⁸)	0.29 (0.8 × 10 ⁹)	0.65 (3.9 × 10 ⁸)	0.27 (1.9 × 10 ⁹)

^a Dielectric constant. ^b Donor number. ^c Acceptor number. ^d The relative fluorescence intensities of dyads referred to those of corresponding diimide-free references. ^e The rate constants of charge separation were calculated on the basis of the following equation: $k_{CS} = (I_0/I - 1)\tau_0^{-1}$ where τ_0 is fluorescence lifetime of diimide-free reference (ca. 1.3 ns).

bridge with these coordinating solvents are not strong enough to alter the absorption spectra of the model compounds.

The steady-state fluorescence spectra of diimide-free references **1a**, **2a**, and **3a** are completely the same in all the solvents, indicating no electronic interaction between ¹ZP* and the respective bridges. The fluorescence spectra of **1a–c** in benzene taken for excitation at 413 nm are shown in Figure 1b. The relative fluorescence intensities

of **1b** and **1c** with respect to that of **1a** are 0.70 and 0.36, respectively. Similarly, the relative fluorescence intensities of PI- and NI-linked models (**2b**, **2c**, **3b**, and **3c**) to those of the acceptor-free models (**2a** and **3a**) were determined in several solvents, and the results are summarized in Table 1. It is evident that the fluorescence quenching of the C-bridged models **3b** and **3c** is commonly observed in all the solvents examined. The relative fluorescence intensities of **3b** and **3c** to those of **3a** are

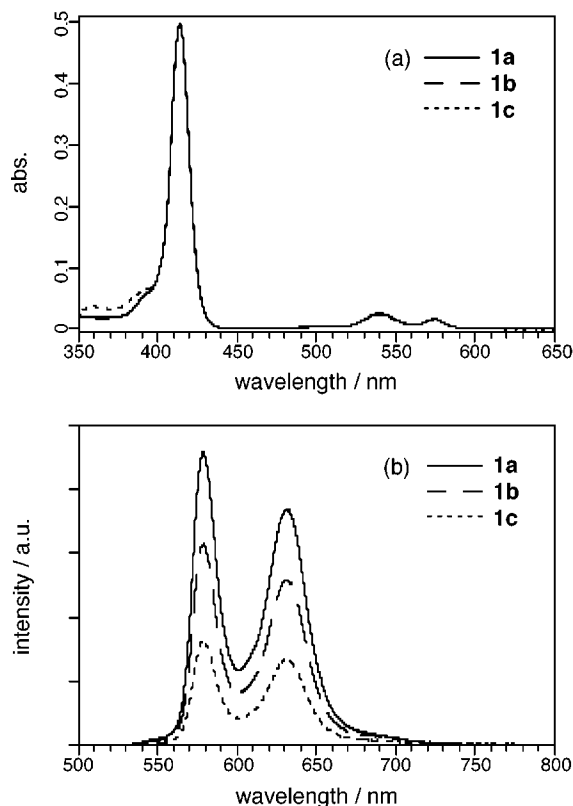


Figure 1. (a) UV-vis absorption and (b) steady-state fluorescence spectra of **1a–c** taken in benzene for excitation at 413 nm.

0.65–0.93 and 0.27–0.57, respectively, and stronger fluorescence quenching in **3c** than **3b** is consistent with charge separation (CS) between $^1\text{ZP}^*$ and diimides, since **NI** is a stronger electron acceptor than **PI**.¹² Practically the same solvent effects were observed for the fluorescence quenching of the N-bridged models **2b** and **2c** (Table 1). In contrast, the solvent effects for the fluorescence quenching in the B-bridged dyads **1b** and **1c** are rather unique. While **1b** and **1c** display fluorescence quenching that is rather similar to those of **3b** and **3c** in benzene, CH_2Cl_2 , THF, and benzonitrile, they display practically no fluorescence quenching in highly electron-pair donating solvents such as DMF, pyridine, and triethylamine.¹³ This contrasting feature is typically shown in Figure 2, where the steady-state fluorescence spectra of **1a–c** and **3a–c** in triethylamine are compared. It was thus suggested that highly electron-pair donating solvents interacts with the Lewis acidic boronate bridge, thereby leading to suppression of the CS reaction between $^1\text{ZP}^*$ and diimide.

Fluorescence Lifetime. The fluorescence lifetimes of these models were determined by the time-correlated single photon counting method in benzene, THF, and DMF, and the results are summarized in Table 2. The fluorescence lifetimes of the acceptor-free molecules **1a**, **2a**, and **3a** were practically the same; 1.40 ns in benzene, 1.46 ns in THF, and 1.54 ns in DMF. The fluorescence decays of **2b**, **2c**, **3b**, and **3c** were found to obey a single-exponential function, and the observed lifetimes were shorter than those of the acceptor-free references **2a** and **3a**, in accordance with the steady-state fluorescence studies. In benzene the fluorescence lifetimes of the B-bridged dyads **1b** and **1c** were 1.18 and 0.57 ns, being shorter than that of **1c**. In THF, the fluorescence decay

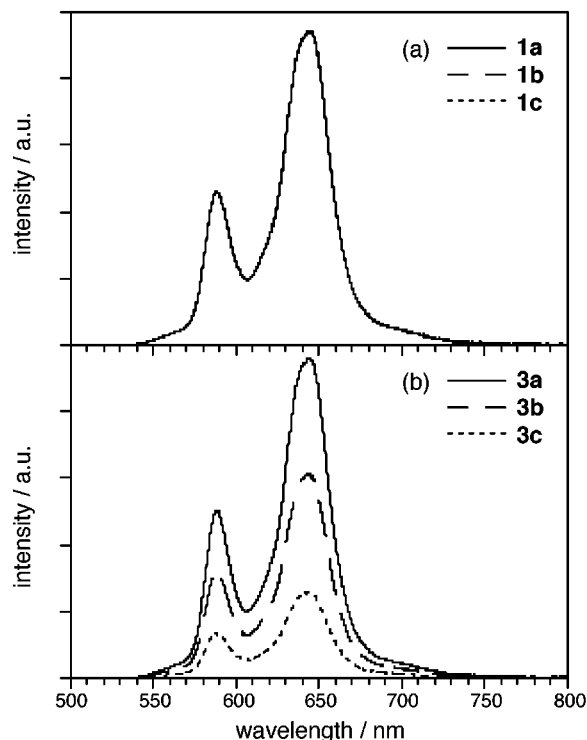


Figure 2. (a) Steady-state fluorescence spectra of **1a–c** and (b) **3a–c** taken in triethylamine for excitation at 422 nm.

Table 2. Fluorescence Lifetime and Lifetime of Photo-generated Ion-pair States

	solvent	τ_F/ns	$k_{\text{CS}}/\text{s}^{-1}$ ^a	$\tau_{\text{IP}}/\text{ns}$	$k_{\text{CR}}/\text{s}^{-1}$ ^b
1b	benzene	1.18	1.3×10^8	40 ± 5	2.5×10^7
	THF	1.36	5.0×10^7	<i>d</i>	
	DMF	1.56			
1c	benzene	0.57	1.1×10^9	13 ± 1 (60%) 290 ± 10 (40%)	7.7×10^7 3.5×10^6
	THF	1.46 (31%) 0.85 (69%)	5.0×10^{8c}	<i>d</i>	
	DMF	1.56		<i>d</i>	
2b	benzene	0.94	3.5×10^8	1.9	5.3×10^8
	THF	0.97	3.3×10^8	<i>d</i>	
	DMF	1.03	3.2×10^8	<i>d</i>	
2c	benzene	0.53	1.2×10^9	190 520	5.3×10^6 1.9×10^6
	THF	0.63	8.8×10^8	<i>d</i>	
	DMF	0.72	7.3×10^8	<i>d</i>	
3b	benzene	1.21	1.1×10^8	84 ± 6	1.2×10^7
	THF	1.34	6.1×10^7	<i>d</i>	
	DMF	1.43	4.6×10^7	<i>d</i>	
3c	benzene	0.49	1.3×10^9	77 ± 16 (66%) 380 ± 100 (34%)	1.4×10^7 2.8×10^6
	THF	0.72	7.1×10^8	<i>d</i>	
	DMF	0.88	4.8×10^8	<i>d</i>	

^a The rate constants of charge separation were calculated on the basis of the following equation: $k_{\text{CS}} = (\tau_F) - 1 - (\tau_F^0) - 1$ where τ_F^0 is fluorescence lifetime of corresponding diimide-free reference; 1.40 ns (benzene), 1.46 ns (THF), and 1.54 ns (DMF). ^b The rate constants of charge recombination were calculated on the basis of the following equation: $k_{\text{CR}} = (\tau_{\text{IP}}) - 1$. ^c k_{CS} was calculated by using $\tau_F = 0.847$ ns. ^d The ion-pair state was not observed (see text).

of **1b** was found to obey single-exponential function with a lifetime of 1.36 ns, while that of **1c** could not be fit with a single exponential function but only with a biexponential function (Table 2). The reason for this biphasic fluorescence decay is not clear in the present stage. In DMF, the fluorescence lifetimes of **1b** and **1c** are both 1.56 ns solution, being practically the same as that of

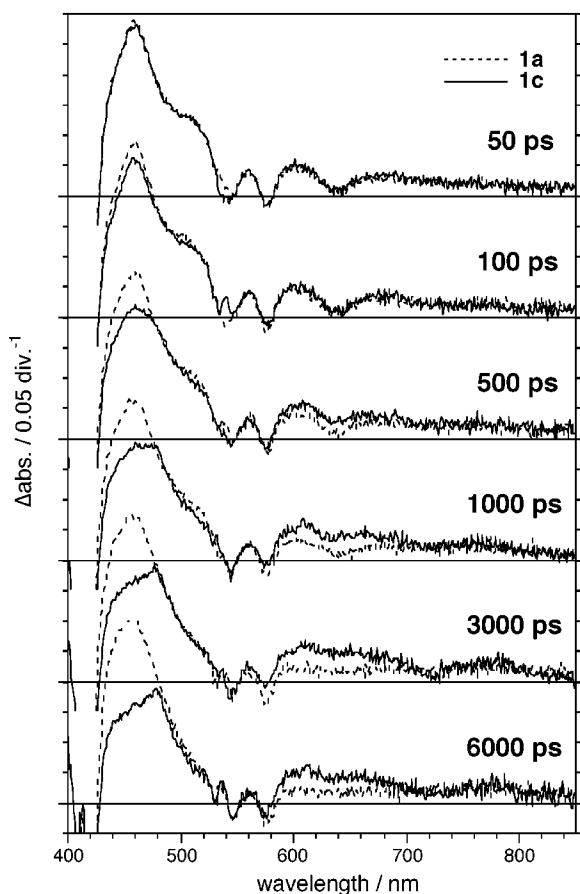


Figure 3. Picosecond time-resolved transient absorption spectra of **1a** (dotted lines) and **1c** (solid lines) taken in benzene for excitation at 532 nm.

the acceptor-free reference **1a**, indicating no fluorescence quenching in accordance with the steady-state fluorescence studies.

Time-Resolved Transient Absorption Spectra.

Both the steady-state and time-resolved fluorescence studies revealed the fluorescence quenching for the acceptor-linked models. The process responsible for the fluorescence quenching has been identified as ET reaction by the time-resolved transient absorption spectroscopy. One of advantages of these models is that the anion radicals of electron acceptors have been spectroscopically well characterized. The anion radical of **PI** exhibits a characteristic sharp absorption band at 721 nm, and the anion radical of **NI** has absorption bands at 480, 650, and 730 nm.¹² Picosecond time-resolved transient absorption spectra of **1a** (dotted line) and **1c** (solid line) in benzene taken for excitation at 532 nm are shown in Figure 3. The spectral changes observed for **1a** correspond to the intersystem crossing from ¹ZP* to ³ZP*.^{12a} In contrast, the transient absorption spectra of **1c** displayed bands at 480 and 610 nm due to **NI**⁻ and a broad band around 650 nm due to **ZP**⁺, providing clear evidence for the formation of ion pair **ZP**⁺–**NI**⁻. Similarly, the transient absorption spectra of **1b** (not shown) exhibited characteristic absorption band due to **PI**⁻ at 721 nm, indicating ion pair (**ZP**⁺–**PI**⁻) formation. Charge recombination (CR) kinetics of the ion pair to the ground state in **1b** measured by monitoring at 721 nm absorbance change followed a single-exponential decay with $\tau = 40 \pm 5$ ns. On the basis of this result, we have determined the rate of CR of **ZP**⁺–**PI**⁻, k_{CR} , to be 2.5×10^7 s⁻¹. On the other

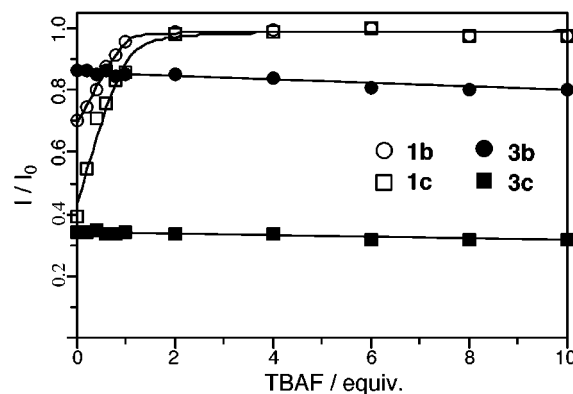


Figure 4. Change of relative fluorescence intensities of **1b** (○), **1c** (□), **3b** (●), and **3c** (■) upon addition of F⁻ in benzene.

hand, the kinetic trace at 480 nm of **1c** showed a biphasic decay with $\tau_1 = 13 \pm 1$ ns (60%) and $\tau_2 = 290 \pm 10$ ns (40%). The similar biphasic decays were observed for the CR reaction of the related triads, which was ascribed to the singlet–triplet intersystem crossing within the ion-pair state on the basis of the external magnetic field effect.¹⁴ Namely, some ion-pair states decayed to the ground-state directly from the singlet manifold, while the rest of the singlet ion-pair states underwent the intersystem crossing to the triplet ion-pair state, which decayed to the ground state after the intersystem crossing to the singlet ion-pair state, thus featuring the biphasic decays. Lifetimes of the ion-pair states (τ_{IP}) in **2b**, **2c**, **3b**, and **3c** were also determined by similar methods, and the results are summarized in Table 2. The similar transient absorption studies conducted in THF revealed only the fast decay of the absorption peak at 460 nm due to ¹ZP* and the characteristic absorption bands due to the ion-pair states could not be detected, indicating faster CR than CS. Acceleration of CR in more polar solvents is relatively common for covalently linked and distance fixed donor–acceptor pairs.^{12a}

Control of Intramolecular ET by F⁻-Coordination.

The results stated above indicate that intramolecular CS reactions in **1b** and **1c** are strongly suppressed in electron-pair donating solvents such as DMF, pyridine, and triethylamine, while such suppression was not observed for the N-bridged and C-bridged dyads. We, thus, examined the intramolecular CS of **1b** and **1c** in the presence of tetra-*n*-butylammonium fluoride (TBAF). We expected the coordination of F⁻ ion at the boronate-bridge, which might lead to a change in electronic communication ability of the bridge. Coordination of F⁻ ion to the boron atom has been studied by ¹¹B NMR. The ¹¹B NMR spectrum of a benzene solution of **1a** showed a broad boron signal around 10 ppm, which was shifted to -14 ppm upon addition of 1 equiv of TBAF. Similar shifts in the ¹¹B NMR were observed also in **1b** and **1c**. The observed high-field chemical shifts are consistent with an electron-rich four-coordinated boronate form.

Figure 4 shows the effects of TBAF addition on the relative fluorescence intensities of **1b**, **1c**, **3b**, and **3c** to those of **1a** and **3a**. It is evident that the fluorescence intensities of **1b** and **1c** increased with an increasing amount of TBAF and restored to the original unquenched levels upon addition of ca. 1 equiv of TBAF, while the fluorescence intensities of **3b** and **3c** are almost insensitive to the amounts of added TBAF. Here it is to be noted that the absorption spectra of **1a**–**c** and the fluorescence

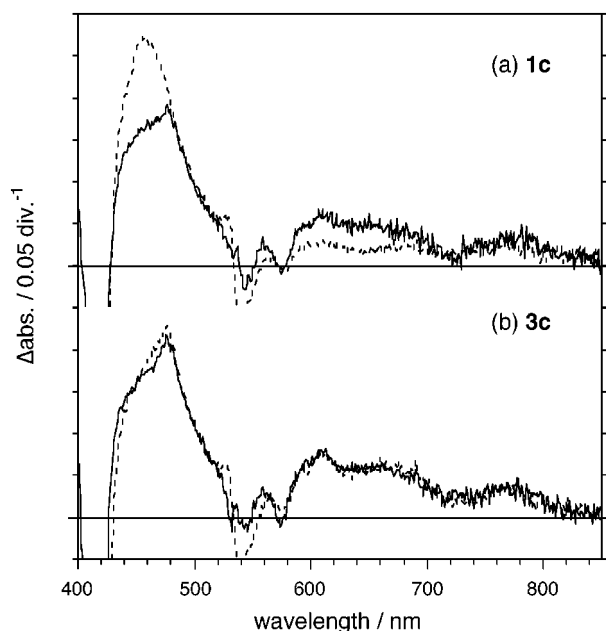


Figure 5. Transient absorption spectra of **1c** (a) and **3c** (b) at 3-ns delay time: solid lines, in the absence of F^- ; dotted lines, in the presence of F^- .

spectrum of **1a** were not affected by the addition of TBAF. The fact that the fluorescence quenching in **1b** and **1c** was suppressed upon the addition of TBAF has been also confirmed by the measurements of the fluorescence lifetime and transient absorption spectra. Namely, the shortened fluorescence lifetimes of free **1b** and **1c** were restored to the unquenched levels (1.56 and 1.58 ns, respectively) upon the addition of more than an equiv. of TBAF in benzene. Transient absorption spectra of **1c** and **3c** at 3-ns delay time in the absence (solid lines) and in the presence of 1.2 equiv. of TBAF (dotted lines) in benzene are shown in Figure 5. In contrast to the ion-pair formation for **1c** in the free form, the transient absorption spectrum of **1c** in the presence of TBAF gave no indication for the ion-pair formation. Essentially the same results were obtained for **1b**. On the other hand, the CS in **3c** was not affected upon the addition of TBAF. This also indicated that the interaction of F^- ion with **ZP** and **NI** has no influence on the ET dynamics.

The N-bridged models **2a–c** were prepared for the purpose of examining the effects of the structural change from a neutral amino-bridge to a positively charged ammonium-bridge upon the intramolecular ET. The fluorescence quenching behaviors in **2b** and **2c** were found to be rather solvent-independent within the range of the solvents used. Probably, the interaction of a piperidine-bridge with solvent has only a subtle effect on the ET dynamics. We also attempted to search pertinent acids that can protonate the piperidine-bridge without interacting with other parts of the models, but we could not find appropriate acids that fulfill our purpose. Strong acids were necessary for protonation of the piperidine bridge in less polar solvents such as THF and benzene, but such acids including as TFA, camphor-4-sulfonic acid, BF_3/OEt_2 , and tri(pentafluorophenyl)borane, preferentially attacked the **ZP** part as revealed by the characteristic spectral changes in the absorption and fluorescence spectra of **2a–c**.

Application of F^- -Coordination Strategy to Control of ET Path Selectivity in PI–ZP–NI Triad 18.

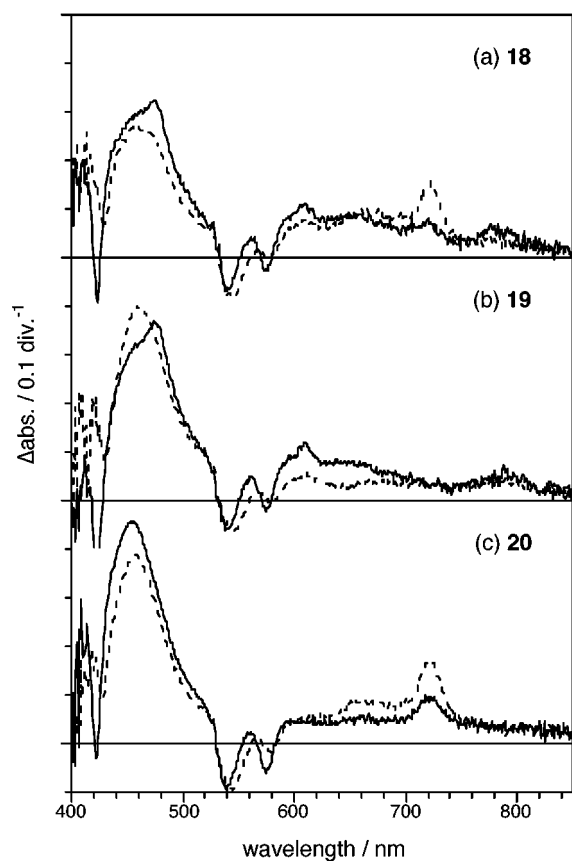
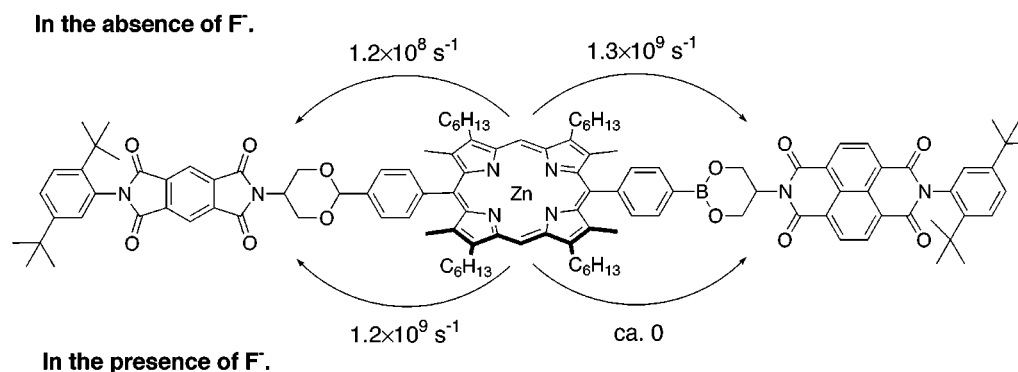


Figure 6. Transient absorption spectra of **18** (a), **19** (b), and **20** (c) at 3-ns delay time: solid lines, in the absence of F^- ; dotted lines, in the presence of F^- .

The high ET path-selectivity in natural RC¹⁵ is an interesting issue not only to understand factors that govern the biological photosynthetic ET reactions but also to construct efficient artificial ET molecular devices. When an “unfavorable” ET path can be made advantageous over a “favorable” ET path without a drop in rate by external input, this will constitute an ET switching device. For this purpose, the “unfavorable” ET path should be simultaneously accelerated. To the best of our knowledge, however, there is no example achieving this type of ET switching. Here, we applied the F^- -coordination strategy to control of ET path-selectivity in triad **18**. Molecular design of **18** is to intend a preferential ET from $^1ZP^*$ to **NI** in the free form but also potential control of ET path selectivity by F^- -coordination at the boronate-ester bridge to switch to a preferential ET from $^1ZP^*$ to **PI**.

In benzene, the fluorescence intensities of **18**, **19**, and **20** relative to that of acceptor-free model **21** were 0.45, 0.44, and 0.89, respectively. This fluorescence quenching suggests intramolecular CS, which has been confirmed by the transient absorption spectra (Figure 6). Absorption peaks due to the radical anions were observed at 475 and 610 nm due to **NI**^{•-} in **19** (Figure 6b) and at 721 nm due to **PI**^{•-} in **20** (Figure 6c), providing clear evidence for formation of the ion pairs, **NI**^{•-}–**ZP**⁺ and **ZP**⁺–**PI**^{•-}, respectively. The transient absorption studies revealed that an excitation of **ZP** with 532-nm laser pulse in **19** and **20** yielded **ZP**⁺–**NI**^{•-} with $\tau = 0.52$ ns and **ZP**⁺–**PI**^{•-} with $\tau = 1.1$ ns, respectively. On the basis of these results, the rates of CS, k_{CS} , have been calculated to be 1.3×10^9 s⁻¹ and 1.2×10^8 s⁻¹ for **19** and **20**, respectively.

Scheme 6. ET Path Selectivity of 18 in the Absence and in the Presence of F⁻ in Benzene

These rates were reasonably in agreement with those determined on the basis of the fluorescence lifetimes (Table 2). Lifetimes of these ion pairs were both longer than 6 ns. Upon the similar laser excitation of **ZP** in **18**, the absorbance due to ¹**ZP*** around 460 nm decayed with $\tau = 0.46$ ns, and the transient absorption spectrum at 3-ns delay time was practically the same as that of **19** except for small absorbance at 721 nm due to **PI**⁻, indicating that CS between ¹**ZP*** and **NI** is dominant in **18**. Comparison of the decay time constants of ¹**ZP*** in **19** and **20** led to conclusion that excitation of **ZP** in **18** leads to formation of **PI**-**ZP**⁺-**NI**⁻ and **PI**⁻-**ZP**⁺-**NI**⁻ in a ratio of 11:1 (Scheme 6).

In the presence of 1.2 equiv of TBAF, the fluorescence intensities of **18**, **19**, and **20** relative to that of **21** were 0.65, 0.98 and 0.72, respectively. The transient absorption spectra of **19** (Figure 6b, dotted line) were practically the same as those of **21** (not shown) from 20 ps to 6 ns delay times, featuring no ET but simple intersystem crossing of ¹**ZP*** to ³**ZP*** with $\tau = 1.5$ ns. Thus, CS between ¹**ZP*** and **NI** in **19** was almost completely suppressed in the F⁻-coordinated form as such for **1c**. Considering similar ET suppression in **18**, its fluorescence quenching should be ascribed to CS between ¹**ZP*** and **PI**. This has been confirmed by the transient absorption spectrum of **18** (Figure 6a, dotted line), which was nearly the same as that of **20** (Figure 6c, dotted line) and showed the appearance of a 721-nm absorption peak due to **PI**⁻. The absorbance changes at 460 nm due to ¹**ZP*** and at 721 nm due to **PI**⁻ in **18** essentially obeyed a single-exponential function with a same lifetime of 0.50 ns. With this result, the rate of the charge separation to **PI** in F⁻-coordinated **18** has been determined to be 1.2×10^9 s⁻¹, which is ca. 10 times faster than that in free **18**. Similar analysis provided $k_{CS} = 6.5 \times 10^8$ s⁻¹ for F⁻-coordinated **20**. It is noteworthy that the CS between ¹**ZP*** and **PI** is significantly accelerated in the presence of F⁻ both in **18** and **20**.

Discussion

The intramolecular ET reaction from ¹**ZP*** to diimide acceptor (**NI** or **PI**) via the boronate-bridge is completely suppressed by the F⁻-coordination on the boron atom. The F⁻-coordination causes changes in many factors that will influence the ET-reaction. Sensitive factors include the geometrical parameters, the energy levels of the ion-pair states, the electronic coupling matrix element between the donor and acceptor, and so on.

A change of trigonal planar boron in sp² conformation to tetrahedral F⁻-coordinated anion in sp³ conformation

induces changes in the geometry of the donor and acceptor. The center-to-center distances between **ZP** and acceptor are estimated by semiempirical MO calculations to be 17.0 and 17.1 Å for free **1b** and **1c** and 16.8 and 16.9 Å for F⁻-coordinated **1b** and **1c**, respectively.¹⁶ The donor-acceptor distances in **3b** and **3c** are similarly estimated to be 16.8 and 17.0 Å. Therefore, the structural changes induced by the F⁻-coordination are subtle and cannot explain the observed ET suppression.

The energy level of the ion-pair states should be changed upon the F⁻-coordination. The one-electron oxidation and reduction potentials of the donor and the acceptors were measured in DMF by cyclic voltammetry: in a free form, $E_{ox}(\mathbf{ZP}) = 0.22$, $E_{red}(\mathbf{PI}) = -1.24$, and $E_{red}(\mathbf{NI}) = -0.98$ V for **1a-c**, $E_{ox}(\mathbf{ZP}) = 0.23$, $E_{red}(\mathbf{PI}) = -1.18$, and $E_{red}(\mathbf{NI}) = -0.94$ V for **2a-c**, and $E_{ox}(\mathbf{ZP}) = 0.22$, $E_{red}(\mathbf{PI}) = -1.18$, and $E_{red}(\mathbf{NI}) = -0.94$ V for **3a-c**, vs ferrocene/ferrocenium ion. In the presence of F⁻, $E_{ox}(\mathbf{ZP}) = 0.22$, $E_{red}(\mathbf{PI}) = -1.24$, and $E_{red}(\mathbf{NI}) = -0.94$ V for **1a-c**, $E_{ox}(\mathbf{ZP}) = 0.22$, $E_{red}(\mathbf{PI}) = -1.19$, and $E_{red}(\mathbf{NI}) = -0.95$ V for **3a-c**. Therefore, it may be concluded that the addition of TBAF had almost no effect on the redox potentials of the respective subunits and the energy levels of the ion-pair states in polar DMF solutions. But estimation of the energy levels of ion-pair states would be more difficult in less polar benzene and THF solutions. Since the center-to-center distances between **ZP** and the boron (9.5 Å) are estimated to be longer than that between the boron and diimide (7.6 Å for **1b** and 7.8 Å for **1c**, respectively), the negative charge on the boron may raise the energy level of the ion-pair state by the overall Coulombic interactions. The magnitude of these electrostatic Coulombic interaction must depend on the dielectric constant of solvents, namely larger in less polar solvents and smaller in more polar solvents. Considering that the CS reaction for covalently linked donor-acceptor molecules are lying at the normal region,¹⁷ the above electrostatic interactions in **1b** and **1c** would decrease k_{CS} value. At the present stage, however, precise estimation of these Coulombic interactions for CS reactions is very difficult.

More importantly, the F⁻-coordination induces changes in the molecular orbitals of the bridge that will alter the electronic coupling matrix element between **ZP** and the diimide (**PI** or **NI**). According to the classical Marcus theory,¹⁹ the ET rate (k_{ET}) depends on Franck-Condon weighted density (FCWD) and the electronic coupling matrix element between a donor and an acceptor (V_{DA}), which is approximately represented as the exchange integral between LUMO of a donor (ϕ_D) and that of an

acceptor (ϕ_A). Furthermore, perturbation in the exchange integral provides the indirect coupling terms in intramolecular ET by using a bridge LUMO (ϕ_B).³ By considering one electron and two LUMO orbitals related to photoinduced ET reaction, a simple representation of V_{AD} is obtained as eq 2

$$k_{ET} = \frac{2\pi}{\hbar} |V_{DA}|^2 (\text{FCWD}) \quad (1)$$

$$V_{DA} = -\langle \phi_D | H | \phi_A \rangle - \frac{\langle \phi_D | H | \phi_B \rangle \times \langle \phi_B | H | \phi_A \rangle}{E(\phi_D) - E(\phi_B)} \quad (2)$$

where the first term corresponds the direct coupling and the second term corresponds to the indirect, superexchange coupling. Semiempirical AM1 SCF MO calculations were performed to estimate the energy levels of HOMOs and LUMOs of **ZP**, diimides (**PI** or **NI**) and the boronate-bridge in the free and F^- -coordinated forms, and the results are summarized in Figure 7. It is apparent that upon the F^- -coordination the rise of bridge LUMO is larger than the corresponding rises of **ZP** and diimide LUMOs, thus resulting in the increase in the energy gap ($\Delta E = E(\phi_D) - E(\phi_B)$), which should suppress the ET reaction. It is also necessary to consider the changes in the exchange integral terms $\langle \phi_D | H | \phi_B \rangle$ and $\langle \phi_B | H | \phi_A \rangle$ upon the F^- -coordination; however, it is difficult to estimate the overlap integral terms in the present stage precisely. The observed unique suppression of CS reaction of **1b** and **1c** in electron-pair donating solvents may be explained in an analogous manner. The interactions of the boronate bridge with such electron-pair donating solvents are not enough to alter the absorption spectral characteristics but seem to be sufficiently large to slow the CS reaction.¹⁹ Moreover, this interpretation has gained more support from our recent results on the intramolecular singlet–singlet and triplet–triplet energy transfer reactions in a boronate-bridged aryl ketone–naphthalene molecule.²⁰ Application of the same F^- -coordination strategy to this dyad led to the complete suppression of triplet–triplet energy transfer from aryl ketone to naphthalene, while singlet–singlet energy transfer from naphthalene to aryl ketone was almost unaffected. Triplet–triplet energy transfer must proceed via the Dexter mechanism,²¹ whose key mechanistic feature is considered to be a simultaneous double electron transfer that must heavily depend on the electronic coupling matrix element between the donor and acceptor.²² On the other hand, the singlet–singlet energy transfer can proceed via dipole–dipole interacting Förster mechanism²³ and thus is free from the F^- -coordination.

ET-path switching in **18** is interesting in view of its distinct path discrimination without a drop in rate. Probably the suppression of ET from $^1ZP^*$ to **NI** may be largely ascribed to the rise of the bridge LUMO orbital,

(19) One of the reviewers pointed out the increase of the reorganization energy upon F^- -coordination as a reason for the suppression of charge separation, since the CS in the F^- -coordinated form or in highly electron-pair donating solvents must involve the dynamic processes such as F^- -ion dissociation or movement away sufficiently to reduce its destabilizing effect on the final charge separated state.

(20) Shiratori, H.; Ohno, T.; Nozaki, K.; Osuka, A. *Chem. Phys. Lett.* **2000**, *320*, 631.

(21) Dexter, D. L. *J. Chem. Phys.* **1953**, *21*, 836.

(22) Closs, G. L.; Piotrowiak, P.; MacInnis, J. M.; Fleming, G. R. *J. Am. Chem. Soc.* **1988**, *110*, 2652.

(23) Förster, T. *Discuss. Faraday Soc.* **1959**, *27*, 7.

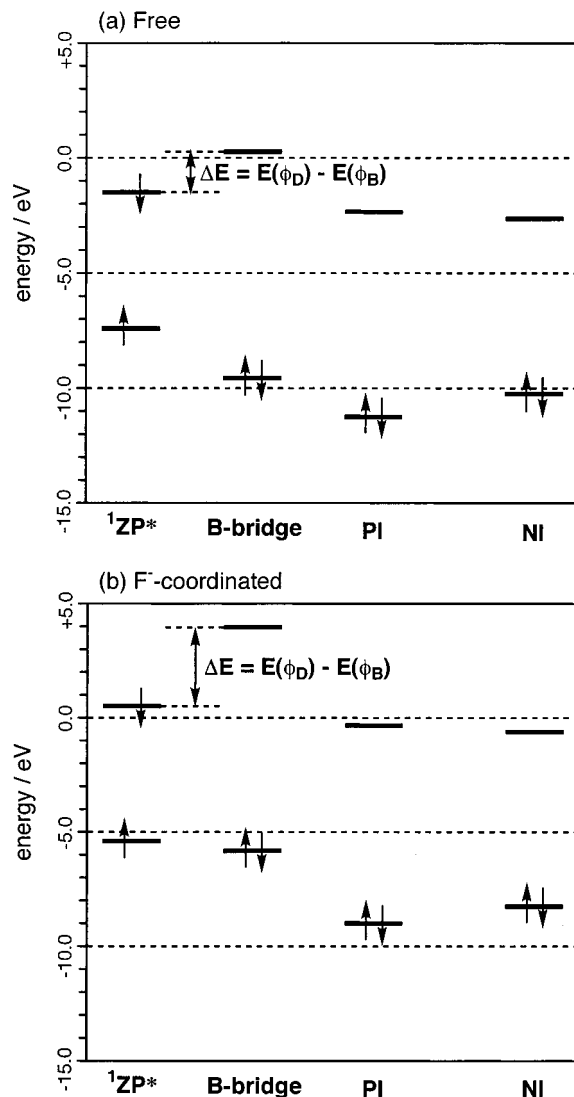


Figure 7. Energy levels of HOMO and LUMO of **ZP**, boronate-bridge and diimides (**PI** and **NI**) estimated by semiempirical MO calculations (MOPAC97, AM1).

but the simultaneous acceleration of the ET from $^1ZP^*$ to **PI** requires other explanation. This acceleration can be explained by considering the electrostatic interaction between negative charge on the F^- -coordinated boron atom and the ion pair $ZP^+ - PI^-$. Interaction between the boronate anion and ZP^+ is attractive and that between the boronate anion and PI^- is repulsive. Since the distance between the boron anion and ZP^+ (9.5 Å) is distinctly shorter than that between the boron anion and PI^- (26.2 Å), the generated negative charge at the boronate bridge in **18** should cause the stabilization of the ion-pair $PI^- - ZP^+ - NI$. This provides larger driving force for the ET reaction from $^1ZP^*$ and **PI**, particularly in nonpolar benzene solution.²⁴ Switching of ET path-selectivity of **18** upon F^- -coordination is summarized in Scheme 6, where the ET from $^1ZP^*$ to **PI** is accelerated about 10-fold in benzene solution.

In summary, the coordination on a neutral boronate-bridge allows a convenient method of controlling in-

(24) The same acceleration should be expected for the CS in **20**, but its acceleration was only half in comparison to the case of **18**. We do not have clear explanation for this discrepancy. A possible cause may be a positional difference of the counteraction between **18** and **20**.

tramolecular ET. The F⁻-coordinated boronate-bridge provides two major effects: (1) the coordinated boronate-bridge has a lifted LUMO orbital that is unfavorable for so-called superexchange interaction between the donor and acceptor, leading to the suppression of the ET, and (2) the negative charge at the boronate-bridge exerts electrostatic interaction with the photogenerated ion-pair state, which is negligible in DMF but significant in benzene. Collectively, almost complete switching of ET-path is achieved in the triad **18**. More detailed mechanistic study and further extension of this strategy to more sophisticated supramolecular systems are now actively in progress in our laboratories.

Experimental Section

Materials and Apparatus. All commercially available materials were used without further purification unless otherwise stated. THF and ether were distilled from sodium-benzophenone ketyl. DMF was dried over molecular sieve 4A for 1 day and distilled under reduced pressure. CH₂Cl₂ was distilled from P₂O₅. Pyridine and triethylamine were dried over KOH for several days and distilled. Toluene was distilled from CaH₂. Anhydrous tetra-*n*-butylammonium fluoride (TBAF) was prepared by heating TBAF·3H₂O at 50 °C for 1 day in vacuo. Solvents used for spectroscopic measurements were all spectrograde. Preparative separations were usually performed by flash column chromatography (Merck, Kieselgel 60H, Art. 7736) and gravity column chromatography (Wako, Wakogel C-200).

¹H NMR (500 MHz) and ¹¹B NMR (160 MHz) spectra were recorded on a JEOL ALPHA-500 FT-NMR spectrometer, and chemical shifts were reported in the δ scale relative to tetramethylsilane for ¹H and to trimethylborate for ¹¹B, respectively. IR spectra were recorded on a JASCO FT/IR-350 spectrometer. Melting points were not corrected. FAB mass spectra were measured on a JEOL HX-110 spectrometer using positive-FAB ionization method and 3-nitrobenzyl alcohol matrix. MALDI-TOF mass spectra were measured on a Shimadzu/KRATOS MALDI 4 spectrometer. UV-vis absorption spectra were recorded on a Shimadzu UV-2400PC UV-vis spectrophotometer. Steady-state fluorescence spectra were recorded on a Shimadzu PF-5300PC spectrometer. Steady-state UV-vis absorption and fluorescence spectra were taken with 1 × 10⁶ M⁻¹ solutions at room temperature. Fluorescence lifetimes were measured with 2 × 10⁻⁵ M solutions by using a picosecond time-correlated single photon counting system for excitation at 532 nm and monitoring at 620 nm emission.²⁵ Picosecond time-resolved transient absorption spectra were measured on Ar-bubbled 2.5 × 10⁻⁵ M solutions by using a mode-locked Nd³⁺:YAG laser system (Continuum PY61C-10, fwhm: 17 ps) with second harmonic output at 532 nm for excitation.²⁶ Nanosecond time-resolved transient absorption spectra were measured by using Q-switched Nd³⁺:YAG laser (Quantel YG 580, fwhm: 5 ns) with second harmonic output at 532 nm for excitation.²⁷

Synthesis. Here, we described the synthetic details of triad **18**. Other synthetic procedures are given in Supporting Information.

N-(2,5-Di-*tert*-butylphenyl)-N-[2-(4-formylphenyl)-1,3-dioxan-4-yl]pyromellitic Diimide (23). PI-appended diol **22** (238 mg, 0.497 mmol), terephthalaldehyde (204 mg, 1.52 mmol), and *p*-toluenesulfonic acid (54 mg, 0.28 mmol) were dispersed in benzene (30 mL), and the reaction mixture was refluxed for 2 h. After the mixture was cooled, the precipitating white solids were collected by filtration and dissolved again in CH₂Cl₂. The CH₂Cl₂ solution was filtered to remove in-

soluble solids and evaporated to give **23** as white solids (255 mg, 0.441 mmol) in 89% isolated yield: mp >300 °C; IR (KBr) ν_{\max} (cm⁻¹) 1722 (C=O of PI) and 1128 (C-O of acetal); ¹H NMR (CDCl₃) 10.06 (s, 1H, CHO), 8.42 (s, 2H, PI-ArH), 7.93 (d, *J* = 8.2 Hz, 2H, *p*-phenylene-ArH), 7.71 (d, *J* = 8.2 Hz, 2H, *p*-phenylene-ArH), 7.57 (d, *J* = 8.5 Hz, 1H, di-*tert*-butylphenyl-ArH), 7.49 (dd, *J* = 8.5, 2.4 Hz, 1H, di-*tert*-butylphenyl-ArH), 6.94 (d, *J* = 2.1 Hz, 1H, di-*tert*-butylphenyl-ArH), 5.72 (s, 1H, acetal-CH), 4.85 (tt, *J* = 11.1, 5.4 Hz, 1H, acetal-CH), 4.69 (t, *J* = 11.1, 2H, acetal-CH₂), 4.27 (dd, *J* = 10.7, 4.9 Hz, 2H, acetal-CH₂), 1.31 (s, 9H, *tert*-butyl), and 1.28 (s, 9H, *tert*-butyl); MS (FAB) *m/z* 594, calcd for C₃₅H₃₄N₂O₇, 594. Anal. Calcd for C₃₅H₃₄N₂O₇, C, 70.69; H, 5.76; N, 4.71. Found: C, 70.7; H, 5.8; N, 4.7.

PI-ZP-B(OH)₂ 25a. Zinc porphyrin **25a** was prepared according to the method for synthesis of zinc porphyrin **7** using PI-appended benzaldehyde **23** (173 mg, 0.30 mmol), 4-formylphenylboronic acid (47 mg, 0.31 mmol), dipyrromethane **5** (266 mg, 0.66 mmol), trichloroacetic acid (12 mg, 73 μmol), and *p*-chloranil (222 mg, 0.90 mmol) to give zinc porphyrin **25a** (108 mg, 74 μmol) in 25% isolated yield. Flash column chromatography on silica gel was performed using CH₂Cl₂ as an eluant: IR (KBr) ν_{\max} (cm⁻¹) 1724 (C=O) 1373 (B-O of B(OH)₂) and 1122 (C-O of acetal); ¹H NMR (CDCl₃) δ 10.19 (s, 2H, meso), 8.47 (s, 2H, PI-ArH), 8.46 (d, *J* = 7.9 Hz, 2H, *p*-phenylene-ArH), 8.25 (d, *J* = 7.6 Hz, 2H, *p*-phenylene-ArH), 8.15 (d, *J* = 7.7 Hz, 2H, *p*-phenylene-ArH), 7.92 (d, *J* = 7.9 Hz, 2H, *p*-phenylene-ArH), 7.59 (d, *J* = 8.5 Hz, 1H, di-*tert*-butylphenyl-ArH), 7.51 (dd, *J* = 8.7, 2.3 Hz, 1H, di-*tert*-butylphenyl-ArH), 6.98 (d, *J* = 2.1 Hz, 1H, di-*tert*-butylphenyl-ArH), 6.06 (s, 1H, acetal-CH), 5.06 (tt, *J* = 10.7, 5.3 Hz, 1H, acetal-CH), 4.89 (t, *J* = 10.8 Hz, 2H, acetal-CH₂), 4.45 (dd, *J* = 10.3, 5.0 Hz, 2H, acetal-CH₂), 3.95 (m, 8H, porphyrin-hexyl-CH₂), 2.48 (s, 6H, porphyrin-methyl), 2.47 (s, 6H, porphyrin-methyl), 2.17 (m, 8H, porphyrin-hexyl-CH₂), 1.74 (m, 8H, porphyrin-hexyl-CH₂), 1.49 (m, 8H, porphyrin-hexyl-CH₂), 1.38 (m, 8H, porphyrin-hexyl-CH₂), 1.33 (s, 9H, *tert*-butyl), 1.31 (s, 9H, *tert*-butyl), 0.91 (t, *J* = 7.3 Hz, 6H, porphyrin-hexyl-CH₃), and 0.91 (t, *J* = 7.0 Hz, 6H, porphyrin-hexyl-CH₃); MS (MALDI-TOF) *m/z* 1451, calcd for C₈₈H₁₀₅N₆O₈BZn, 1449. Anal. Calcd for C₈₈H₁₀₅N₆O₈Zn, C, 72.84; H, 7.29; N, 5.79. Found: C, 73.0; H, 7.4; N, 5.8.

5-(4-Dihydroxyborylphenyl)-15-[4-(5,5-dimethyl-1,3-dioxan-2-yl)phenyl]-2,8,12,18-tetra-*n*-hexyl-3,7,13,17-tetramethylporphyrinatozinc(II) (25b). Zinc porphyrin **25b** was prepared according to the method for synthesis of zinc porphyrin **7** using 4-(5,5-dimethyl-1,3-dioxan-2-yl)benzaldehyde **24** (67 mg, 0.30 mmol), 4-formylphenylboronic acid (46 mg, 0.31 mmol), dipyrromethane **5** (228 mg, 0.67 mmol), trichloroacetic acid (10 mg, 61 μmol), and *p*-chloranil (221 mg, 0.90 mmol) to give zinc porphyrin **25b** (48.6 mg, 45 μmol) in 15% isolated yield. Flash column chromatography on silica gel was performed using 1.5% methanol in CH₂Cl₂ as an eluant: IR (KBr) ν_{\max} (cm⁻¹) 1373 (B-O of B(OH)₂) and 1105 (C-O of acetal); ¹H NMR (CDCl₃) δ 10.12 (s, 2H, meso), 8.11 (d, *J* = 7.8 Hz, 2H, *p*-phenylene-ArH), 8.10 (d, *J* = 7.6 Hz, 2H, *p*-phenylene-ArH), 8.08 (d, *J* = 7.8 Hz, 2H, *p*-phenylene-ArH), 7.89 (d, *J* = 8.0 Hz, 2H, *p*-phenylene-ArH), 5.77 (s, 1H, acetal-CH), 3.99 (d, *J* = 10.7 Hz, 2H, acetal-CH₂), 3.92 (m, 8H, porphyrin-hexyl-CH₂), 3.87 (m, 8H, porphyrin-hexyl-CH₂), 2.45 (s, 6H, porphyrin-methyl), 2.41 (s, 6H, porphyrin-methyl), 2.17 (m, 8H, porphyrin-hexyl-CH₂), 1.74 (m, 8H, porphyrin-hexyl-CH₂), 1.50 (s, 3H, acetal-CH₃), 1.50 (m, 8H, porphyrin-hexyl-CH₂), 1.41 (m, 8H, porphyrin-hexyl-CH₂), 0.96 (s, 3H, acetal-CH₃), 0.93 (t, *J* = 7.3 Hz, 6H, porphyrin-hexyl-CH₃), and 0.92 (t, *J* = 7.3 Hz, 6H, porphyrin-hexyl-CH₃); MS (FAB) *m/z* 1076, calcd for C₆₆H₈₇N₄O₄BZn, 1075. Anal. Calcd for C₆₆H₈₇N₄O₄BZn, C, 73.63; H, 8.14; N, 5.20. Found: C, 74.1; H, 8.2; N, 5.1.

Triad PI'-ZP-NI 18. Triad **18** was prepared according to the method for the synthesis of **1c** using PI-ZP-B(OH)₂ **25a** (73.7 mg, 51 μmol) and NI-appended diol **26** (27.2 mg, 52 μmol) to give triad **18** (85.0 mg, 44 μmol) in 86% isolated yield: IR (KBr) ν_{\max} (cm⁻¹) 1720 (C=O of PI and NI), 1315 (B-O of boronate) and 1130 (C-O of acetal). ¹H NMR (CDCl₃) δ 10.19 (s, 2H, meso), 8.88 (d, *J* = 7.6 Hz, 2H, NI-ArH), 8.86

(25) Yamazaki, I.; Tamai, N.; Kume, H.; Tsuchiya, H.; and Oba, K. *Rev. Sci. Instrum.* **1985**, *56*, 1187.

(26) Yoshimura, A.; Nozaki, K.; Ikeda, N.; Ohno, T. *J. Phys. Chem.* **1996**, *100*, 1630.

(27) Ohno, T.; Nozaki, K.; Haga, M. *Inorg. Chem.* **1991**, *30*, 767.

(d, $J = 7.6$ Hz, 2H, NI-ArH), 8.46 (s, 2H, PI-ArH), 8.24 (d, $J = 7.6$ Hz, 2H, *p*-phenylene-ArH), 8.15 (d, $J = 6.4$ Hz, 2H, *p*-phenylene-ArH), 8.13 (d, $J = 7.9$ Hz, 2H, *p*-phenylene-ArH), 7.93 (d, $J = 7.9$ Hz, 2H, *p*-phenylene-ArH), 7.63 (d, $J = 8.9$ Hz, 1H, di-*tert*-butylphenyl-ArH), 7.60 (d, $J = 8.9$ Hz, 1H, di-*tert*-butylphenyl-ArH), 7.51 (dd, $J = 8.9$, 2.1 Hz, 1H, di-*tert*-butylphenyl-ArH), 7.51 (dd, $J = 8.7$, 2.3 Hz, 1H, di-*tert*-butylphenyl-ArH), 7.04 (d, $J = 2.1$ Hz, 1H, di-*tert*-butylphenyl-ArH), 6.98 (d, $J = 2.1$ Hz, 1H, di-*tert*-butylphenyl-ArH), 6.06 (s, 1H, acetal-CH), 5.90 (tt, $J = 10.4$, 5.2 Hz, 1H, boronate-CH), 5.21 (t, $J = 10.2$ Hz, 2H, boronate-CH₂), 5.05 (tt, $J = 10.9$, 5.3 Hz, 1H, acetal-CH), 4.88 (t, $J = 10.7$ Hz, 2H, acetal-CH₂), 4.45 (dd, $J = 10.1$, 4.9 Hz, 2H, acetal-CH₂), 4.41 (dd, $J = 10.1$, 4.9 Hz, 2H, boronate-CH₂), 3.97 (m, porphyrin-hexyl-CH₂), 2.49 (s, 6H, porphyrin-methyl), 2.47 (s, 6H, porphyrin-methyl), 2.19 (m, 8H, porphyrin-hexyl-CH₂), 1.75 (m, 8H, porphyrin-hexyl-CH₂), 1.49 (m, 8H, porphyrin-hexyl-CH₂), 1.39 (m, 8H, porphyrin-hexyl-CH₂), 1.35 (s, 9H, *tert*-butyl), 1.33 (s, 9H, *tert*-butyl), 1.31 (s, 9H, *tert*-butyl), 1.29 (s, 9H, *tert*-butyl), 0.92 (t, $J = 7.3$ Hz, 6H, porphyrin-hexyl-CH₃), and 0.92 (t, $J = 7.3$ Hz, 6H, porphyrin-hexyl-CH₃); MS (MALDI-TOF) m/z 1946, calcd for C₁₁₉H₁₃₃N₈O₁₂BZn, 1941. Anal. Calcd for C₁₁₉H₁₃₃N₈O₁₂BZn: C, 73.54; H, 6.90; N, 5.77. Found: C, 73.5; H, 6.9; N, 5.8.

Dyad ZP–NI^I 19. Reference dyad **19** was prepared according to the method for the synthesis of **1c** using ZP–B(OH)₂ **25b** (33.5 mg, 31 μmol) and NI-appended diol **26** (16.4 mg, 31 μmol) to give dyad **19** (36.9 mg, 24 μmol) in 76% isolated yield: IR (KBr) ν_{\max} (cm⁻¹) 1711 (C=O of NI), 1313 (B–O of boronate) and 1103 (C–O of acetal); ¹H NMR (CDCl₃) δ 10.18 (s, 2H, meso), 8.87 (d, $J = 7.6$ Hz, 2H, NI-ArH), 8.84 (d, $J = 7.3$ Hz, 2H, NI-ArH), 8.24 (d, $J = 7.6$ Hz, 2H, *p*-phenylene-ArH), 8.13 (d, $J = 7.9$ Hz, 2H, *p*-phenylene-ArH), 8.11 (d, $J =$

7.9 Hz, 2H, *p*-phenylene-ArH), 7.89 (d, $J = 7.9$ Hz, 2H, *p*-phenylene-ArH), 7.63 (d, $J = 8.5$ Hz, 1H, di-*tert*-butylphenyl-ArH), 7.51 (dd, $J = 8.7$, 2.3 Hz, 1H, di-*tert*-butylphenyl-ArH), 7.04 (d, $J = 2.1$ Hz, 1H, di-*t*-butylphenyl-ArH), 5.89 (tt, $J = 10.2$, 5.0 Hz, 1H, boronate-CH), 5.77 (s, 1H, acetal-CH), 5.19 (t, $J = 10.4$, 2H, boronate-CH₂), 4.39 (dd, $J = 9.8$, 5.1 Hz, 2H, boronate-CH₂), 3.99 (d, $J = 10.7$ Hz, 2H, acetal-CH₂), 3.96 (t, $J = 7.6$ Hz, 4H, porphyrin-hexyl-CH₂), 3.95 (t, $J = 8.2$ Hz, 4H, porphyrin-hexyl-CH₂), 3.87 (d, $J = 10.4$, 2H, acetal-CH₂), 2.48 (s, 6H, porphyrin-methyl), 2.46 (s, 6H, porphyrin-methyl), 2.18 (m, 8H, porphyrin-hexyl-CH₂), 1.75 (m, 8H, porphyrin-hexyl-CH₂), 1.51 (s, 3H, acetal-CH₃), 1.50 (m, 8H, porphyrin-hexyl-CH₂), 1.39 (m, 8H, porphyrin-hexyl-CH₂), 1.36 (s, 9H, *tert*-butyl), 1.29 (s, 9H, *tert*-butyl), 0.94 (s, 3H, acetal-CH₃), 0.92 (t, $J = 6.6$ Hz, 6H, porphyrin-hexyl-CH₃), and 0.92 (t, $J = 7.3$ Hz, 6H, porphyrin-hexyl-CH₃); MS (MALDI-TOF); m/z 1568, calcd for C₉₇H₁₁₅N₆O₈BZn, 1567. Anal. Calcd for C₉₇H₁₁₅N₆O₈BZn: C, 74.24; H, 7.39; N, 5.36. Found: C, 74.3; H, 7.5; N, 5.4.

Acknowledgment. This work was partly supported by a Grant-in Aid for Scientific Research (No. 09440217) from the Ministry of Education, Science, Sports and Culture of Japan and by CREST (Core Research for Evolutional Science and Technology) of Japan Science and Technology Corporation (JST).

Supporting Information Available: Detailed synthetic procedures of the other new compounds appearing in this paper. This material is available free of charge via the Internet <http://pubs.acs.org>.

JO001281W